Humidity Sensors: A Review

Article *in* Sensor Letters · January 2005

DOI: 10.1166/sl.2005.001

CITATIONS
330

READS
22,467

2 authors:

Chia-Yen Lee
National Pingtung University of Science and Technology
94 PUBLICATIONS **3,784** CITATIONS
SEE PROFILE

Gwo-Bin Lee
National Tsing Hua University
586 PUBLICATIONS **14,350** CITATIONS
SEE PROFILE

SENSOR LETTERS
Vol. 3, 1–14, 2005

REVIEW

Humidity Sensors: A Review

Chia-Yen Lee[1] and Gwo-Bin Lee[2,*]

[1] *Department of Mechanical and Automation Engineering, Da-Yeh University, Changhua, Taiwan 515*
[2] *Department of Engineering Science, National Cheng Kung University, Tainan, Taiwan 701*

(Received: 7 October 2004. Accepted: 17 December 2004)

CONTENTS

1. OVERVIEW

Humidity is one of the most commonly measured physical quantities and is of great importance in a wide variety of commercial and industrial applications, including those associated with building ventilation control, clean rooms in the semiconductor and automotive industries, environmental chambers for the testing of electronics, industrial drying, and process monitoring in the chemicals, electronics, food/beverage, pharmaceutical, cosmetics and biomedical analysis industries.

Humidity is defined as a measure of the water vapor present in a gas. Two common parameters in associated with humidity measurement are absolute humidity and relative humidity. Absolute humidity is referred to a measure of the mass of water vapor in a unit volume. Similarly, relative humidity is defined as the ratio of the water-vapor pressure present to the water-vapor pressure required for saturation at a given temperature. The relative humidity is related to ambient temperature. Water vapor is a natural component of air, and the relative humidity (RH) of the water vapor and air mixture is defined as the ratio of the mass of water vapor in a unit volume compared to the mass of water vapor which that volume could hold if the vapor were saturated at the mixture temperature. RH is typically expressed as:

$$\mathrm{RH} = \frac{P_w}{P_s} \times 100\% \tag{1}$$

where P_w and P_s are the vapor and saturation pressures, respectively.

Another commonly measured parameter associated with relative humidity is the dew point, T_d (°C), which defines the temperature below which condensation of water occurs. The expressions and definitions of the wet-bulb and dew-point temperatures are plotted in Figure 1. Having measured the values of P_w and P_s, it is clear that the corresponding relative humidity value can be determined from Eq. 1.

Humidity measurement is generally conducted using a psychrometer. Figure 2 presents a schematic illustration of a psychrometer (IMAG-DLO, IMax) comprising two thermometers,[1] which measure the dry-bulb and wet-bulb temperatures, respectively. The vapor pressure, P_w, can then be calculated from:

$$P_w = P_s - P_t A(T_{wet} - T_{air}) \tag{2}$$

where P_s is the saturation vapor pressure at T_{air} (dry-bulb temperature), P_t is the total medium pressure, T_{wet} is the measured wet-bulb temperature, and A is the psychrometer constant, which is a function of the psychrometer geometry and the air flow rate.[2]

It can be shown that the approximated thermodynamic psychrometer constant (A) has a value of 5.68 at 0 °C, 6.44∼6.46 at 20 °C, 6.28∼6.45 at 40 °C, and 5.63∼6.43 at 60 °C. This constant is temperature-dependent and varies more greatly with relative humidity under high temperature conditions. The thermodynamic properties are calculated using the perfect-gas relationships of moist air. Although psychrometers have the disadvantage of requiring regular maintenance, their operational principle is simple and unique. Hence, their use is invaluable when calibrating other air humidity sensors.[3]

*Corresponding author; E-mail: gwobin@mail.ncku.edu.tw

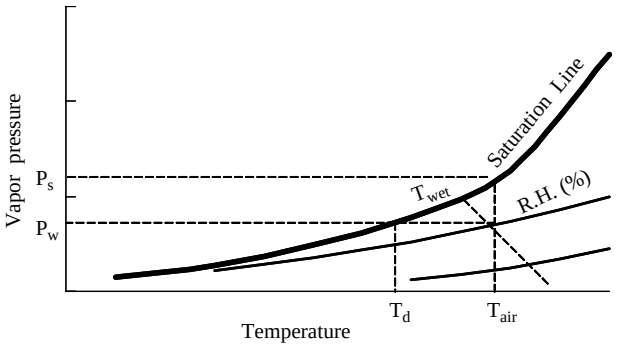

Figure 1. Psychrometric chart, where T_{air} is the ambient air temperature. If the temperature drops below the dew point, T_d (°C), condensation of water occurs.

This paper reviews the transduction techniques of various state-of-the-art humidity sensors, including (1) optical, (2) gravimetric, (3) capacitive, (4) resistive, (5) piezoresistive, and (6) magnetoelastic sensors.

2. OPTICAL HUMIDITY SENSORS

Fiber-optic humidity sensors are based on the colorimetric interaction of materials immobilized on the surface of the fiber core or its cladding in the humidity-sensing section. The sensing mechanism relies on a humidity-induced refractive index change in the materials, which causes the transmitted optical intensity through the sensing section to vary as a function of the relative humidity.

Kharaz and Jones[4] presented an optical-fiber humidity sensing system based on the colorimetric interaction of cobalt chloride with water molecules. As shown schematically in Figure 3, a 50 mm length of the fiber cladding was removed and replaced by a cobalt chloride-gelatin thin film. While maintaining a constant temperature of 36 °C, it was shown that variations of relative humidity were reflected as changes in the spectral absorption of the sensor in the wavelength range of 600–740 nm. Meanwhile, a second wavelength beyond this range served as an intensity reference. The relative intensity of the signals was obtained by dividing the intensity of the light at the 670 nm wavelength by that at a wavelength of 850 nm. The average humidity sensitivity was found to be 0.001∼0.007 a.u./%RH.

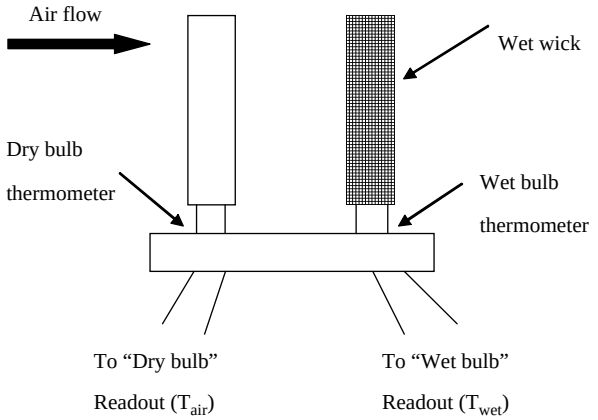

Figure 2. Schematic illustration of psychrometer. The wet bulb thermometer is kept moist by a cotton wick placed in a water reservoir, and is used to measures T_{wet}. The dry bulb thermometer measures the ambient air temperature T_{air}.[1]

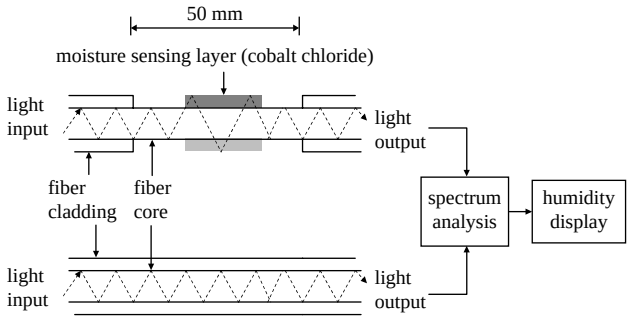

Figure 3. Construction and operation of an optical humidity sensor. A 50 mm length of the fiber cladding is removed and replaced by a cobalt chloride-gelatin thin film. When the temperature is maintained at 36 °C, a change of relative humidity affects the spectral absorption of the sensor in the wavelength region 600–740 nm. Meanwhile, a second wavelength outside this region provides an intensity reference. The relative intensity of the signals is obtained by dividing the intensity of the light at 670 nm by that of the light at 850 nm. The average humidity sensitivity is 0.001∼0.007 a.u./%RH at different operating regions.[4]

In an alternative approach, a hydrophilic gel (agarose) was deposited on the thinner zone of a biconically tapered single-mode optical fiber.[5] Using this arrangement, 6.5 dB of attenuation was obtained as the relative humidity was changed from 30% to 80%. However, an apparent hysteresis of 0.5 dB was also observed.

Optical techniques also make use of the absorption wavelength of water. When light is passed through a gas, the absorption of certain wavelengths gives rise to a significant change in both the polarization and the amplitude of the incident optical signal. For example, Schirmer et al.[6] presented a fiber-coupled diode laser absorption spectrometer modulated with 7.50 ± 0.01 GHz for the detection of humidity at different frequencies. Once the background noises had been subtracted, it was determined that the absorption signals were proportional to the humidity volume fractions with a sensitivity of 0.01105 V/ppm.

Films of PVA (polyvinyl alcohol)/H_3PO_4 containing dyes (CV ⟨crystal violet⟩/MB ⟨methylene blue⟩) were applied to optical humidity sensing by Somani et al.[7] An apparent spectrum shift was observed when the relative humidity was increased from 9% RH to 100% RH.

Ha et al. presented a mechanical-optoelectronic humidity sensor comprising an LED (light-emitting device), a photodiode, and a mechanical system.[8] In this device, one end of the hair bunch is fixed, while the other end is connected to a thin metal sheet, which contains a window and is connected to a spiral spring. A humidity change causes a contraction or expansion of the hair, which then pulls the metal sheet up or down. The motion of the sheet relative to the fixed metal target changes the window area, which in turn causes a change in the LED light intensity detected at

the photodiode and a corresponding change in the output photocurrent. Compared to capacitive or resistive humidity sensors, the mechanical-optoelectronic humidity sensor demonstrates an improved long-term stability and a reduced temperature dependency.[8]

Gupta and Ratnanjali[9] reported a fiber-optic humidity sensor based on the moisture-dependent absorption of light by using a phenol red doped polymethylmethacrylate (PMMA) film over a small portion of the core of the plastic clad silica (PCS) fiber with a lower refractive index. An ingenious U-shaped probe was designed to decrease the angle of incidence of the ray at the core-film interface in the bent region and hence to increase the transmission of light from the core to the sensor. The response time of this sensor is about 5 sec while operating from 20 to 80% RH, which demonstrated a rapid response for optical humidity sensors. Shukla et al.[10] reported nano-structured magnesium-oxide films by using sol–gel techniques to sense the moisture surrounding a similar U-shaped probe. In their study, optical fibers were utilized to sense adsorption of humidity on nanosize MgO films coated on U-shaped glass rods while a light guide received the input optical power at one end and delivered the output optical power at the other end. The change in the output optical power was shown to be highly related with the humidity. Besides, polymer-based optode membranes doped with fluorescence were also used for sensing of relative humidity, and demonstrated a high detection resolution up to 0.56%.[11, 12]

Sorli et al.[13] developed optical humidity sensors based on the cooled mirror principle using optical detection techniques. The sensors were composed of a reflective sensor and a Peltier module, which controlled the temperature to reach the dew point and to evaporate the condensate water. A LED and a photo-detector were used to measure the water droplets. The water contents ranging between 80 and 95% were measured with high accuracy. Drew et al.[14] demonstrated a humidity sensor using vapor-luminescent platinum (II) double salt materials. Luminescence spectra for platinum (II) double salt materials showed that the intensity and the wavelength maximum corresponded to the concentration of water vapor surrounding the materials. The excitation light was generated by mounting a blue LED at the end of one of the bifurcated fibers and the collection end of the bifurcated fiber was connected to a spectrophotometer for the analysis of the spectrum of the luminescent platinum (II) double salt materials. Thus water vapor could be detected successfully using this approach.

Photo-acoustic (PA) humidity sensing systems using laser diodes were also developed.[15] Due to the dependence of the photo-acoustic signals on various physical and chemical properties of the measured gas samples, minimum detectable concentration of water vapor up to sub-ppm level could be achieved using the developed diode-laser-based PA water vapor detection systems (DPWDS).

Although optical humidity sensors have a high sensitivity, several drawbacks hinder their practical application, including hysteresis, typically varying from 0.5% to 1% RH, their bulky nature, the requirement for frequent mirror decontamination, their instability under continuous use, a relatively high power consumption, the requirement for some form of temperature compensation mechanism if precise humidity measurements are to be obtained, and finally, their relatively high costs. Notwithstanding these limitations, the capability of optical humidity sensors to track low-level moisture levels is superior to that of their counterparts and hence, these devices are generally employed in laboratory environments. Table I summarizes the design and materials used for various optical humidity sensing systems.

3. GRAVIMETRIC HUMIDITY SENSORS

Surface acoustic wave (SAW) devices have been widely used in humidity measurement applications. Wohltjen presented a SAW sensor with the ability to measure vapor

Table I. Overview of transduction techniques for optical humidity sensors.

Year	Authors	Design	Materials	Output	Remarks	Ref.
1995	Kharaz and Jones	Fiber-optic	$CoCl_2$	Intensity of light	Surface-plasma-based device	[4]
2000	Bariáin et al.	Fiber-optic	Agarose gel	Optical power	Sol–gel deposition	[5]
	Schirmer et al.	Spectrometer	—	Spectrometer	Frequency modulation	[6]
	Ha et al.	Movable window	Black hair	Voltage	Photodiode for conversion	[8]
	Choi and Shuang	Fluorescent	Optode membrane	Transmission	Fluorescent optosensor	[12]
2001	Somani et al.	UV-VIS spectra	Complex-forming dyes	Absorbance	Charge transfer complex-forming dyes	[7]
	Gupta and Ratnanjali	Fiber-optic	PMMA	Transmission	U-shaped probe	[9]
	Bedoya et al.	Fluorescent	Optode membrane	Transmission	Fluorescent optosensor	[11]
2002	Sorli et al.	Optical reflection	Peltier device	Voltage	Dew point sensing	[13]
2003	Bozóki et al.	Fabry-Pérot interferometer	Photoacoustic cell	Wavenumber	Photoacoustic	[15]
2004	Shukla et al.	Fiber-optic	Nano-like MgO	Transmission	U-shaped probe	[10]
	Drew et al.	Luminescence spectra	Pt(II) double salt materials	Wavelength	Vaporluminescent	[14]

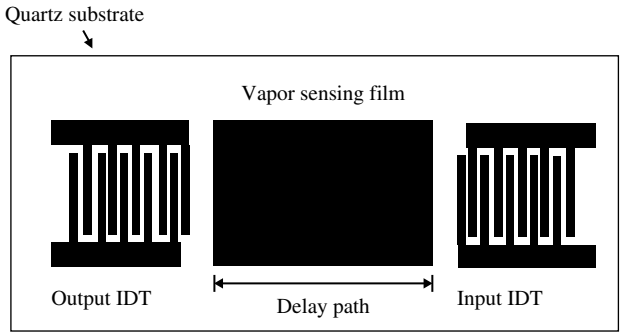

Figure 4. Schematic illustration of a SAW sensor. The sensor creates a series of SAWs which travel across the sensing film to the output IDT where they are converted back into an electrical signal.[17]

(humidity) with a greater sensitivity than bulk wave sensors.[16] In a SAW sensor, surface acoustic waves are launched along the delay path of the SAW sensor (Fig. 4) via the reverse piezoelectric effect when an RF signal is applied at the center frequency to the input interdigital transducer (IDT). This creates a series of SAWs, which travel across the vapor sensing film to the output IDT, where they are then converted back to an electrical signal.[17] Hence, the relative change (Δv) in the SAW phase velocity (v_0) caused by the mass density changes induced by vapor absorption can be given approximately as:

$$\frac{\Delta v}{v_0} = -\frac{\pi h v_0^2}{2\lambda}\Delta\rho(A_x^2 + A_y^2 + A_z^2) \tag{3}$$

where h is the thickness of the film, $\Delta\rho$ is the change of the mass density, λ is the acoustic wavelength, and Ai ($i = x$, y, or z) are the normalized displacement amplitudes of the SAW.

Hence, the relative humidity can be determined by measuring the relative change of the phase velocity. The relative changes in the phase velocity and frequency are related by the expression given in Eq. 4[18]

$$\frac{\Delta v}{v_0} = \frac{\Delta f}{f_0} \tag{4}$$

where Δf is the frequency shift caused by the vapor absorption and f_0 is the SAW frequency.

A typical SAW humidity sensor is operated using RF amplifiers with a coupler. The oscillation frequency is monitored using a frequency counter.[19] Although these sensors are relatively sensitive, oscillator instability can pose problems in practical applications. Typically, the ratio $\Delta f/f_0$ of the SAW humidity sensor increases from 0 to 22 ppm as the relative humidity changes from 0% RH to 85% RH when a polyethynylfluorenol (PEFL) sensing membrane is used. It is clear that this sensitive membrane yields a high humidity sensitivity. It is noted that cellulose acetate films,[20] hexamethyldisiloxane (HMDSO) and polymer-like hydrogenated amorphous carbon (a-C:H) films,[21] Al_2O_3 ceramic thin film,[22] polyvinyl alcohol (PVA) film[23] and other polymer films[24] have also been reported as sensitive membranes.

Radeva et al. presented an alternative type of gravimetric humidity sensor.[25] In his study, the sensitive detection capability ($10^{-8}\sim10^{-11}$ g) of a quartz crystal microbalance (QCM) was exploited to perform the characterization of vapors. The operation of this sensor is based on the shift of the resonant frequency (Δf) away from the resonant driving frequency (f_r) when an additional mass (Δm) is deposited on the sensing film. This dependency can be expressed as:

$$\frac{\Delta f}{f_r} = -\frac{\Delta m}{M} \tag{5}$$

where M is the mass of the quartz piezoelectric substrate. Thin (0.12 μm) fullerene layers are deposited on either side of the QCM to serve as adsorptive layers for water molecules. The mass of water molecules absorbed by the fullerene layer causes a decrease of the resonant frequency. The number of water molecules absorbed depends on their concentration in the environment (i.e. the relative humidity). These sensors also demonstrate a quick response (1.0 sec) to cyclic changes in the air humidity.

Glück et al. proposed a cantilever-type resonator utilizing a stratified structure with a piezoelectric polymer layer (polyvinyl-difluorene, PVDF).[26] A cantilever vibration is induced by the expansion or contraction which takes place when an electrical signal is applied to the electrodes placed on either side of the PVDF. The adsorption of water vapor results in a change of the mass, Δm, which causes a shift in the resonant frequency of the beam. In the range 0–90% RH, a frequency shift of 30 Hz was observed at a resonant frequency of 1.39 kHz.[26]

In general, gravimetric humidity sensors provide a high sensitivity, a rapid response time and a simple experimental setup. However, they generally require expensive driving and detection electronics. Table II summarizes the design and materials used for various gravimetric humidity sensing systems.

4. CAPACITIVE HUMIDITY SENSORS

Approximately 75% of the humidity sensors on the market today are based on the capacitive technique.[3] Capacitive humidity sensors offer several advantages, including very low power consumption and high output signals. Using these sensors, the ambient relative humidity level is measured by detecting moisture-induced changes in the dielectric constant of a hygroscopic layer. Typically, capacitive humidity sensors are composed of two interdigitated electrodes (IDE) covered by a dielectric layer, which is sensitive to humidity changes (Fig. 5). The measured capacitance values demonstrate a nonlinear relationship with the relative humidity. Story et al.[27] employed a polyimide film (DuPont 5878) as the moisture sensitive layer. Although a thin polyimide film (2 μm) yields a higher sensitivity (27 fF/%RH), serious hysteresis occurs at high values of RH. Hysteresis is a common problem for virtually

Table II. Overview of transduction techniques for gravimetric humidity sensors.

Year	Authors	Design	Materials	Output	Remarks	Ref.
1984	Wholtjen	SAW	Piezoelectric materials	Frequency	Piezoelectric effect	[16]
1994	Glück et al.	Cantilever	PVDF	Frequency	Resonant sensor	[26]
1996	Vetelino et al.	SAW, IDE	Al, ST-quartz	Frequency	Dew point detection	[17]
1997	Caliendo et al.	SAW, IDE	CIMs	Frequency	Study of materials	[18]
	Galipeau et al.	SAW, IDE	Polyimide, ST-quartz	Frequency	SAW sensors	[19]
	Radeva et al.	QCM, thick film	Fullerene	Frequency	Study of materials	[25]
1999	Braga et al.	SAW, IDE	Cellulose acetate film	Frequency	Thick-film technology	[20]
2000	Jain et al.	Magnetoacoustic, IDE	Ferromagnetics	Frequency	Remote sensing	[22]
	Penza and Cassano	QCM, IDE	Polymers (PVA)	SAW-phase	Hybrid PLL electronics	[23]
2004	Bruno et al.	STW resonator, IDE	HMDSO, a-C:H films	Frequency	Surface transverse acoustic wave	[21]

all kinds of capacitive humidity sensors due to the slower diffusion time of moisture sensitive films while dehumidifying.

Other materials such as PMMA,[28,29] porous ceramics,[30–32] porous silicon,[33–36] porous silicon carbide[37] and hygroscopic polymers[27,38] have also been utilized as humidity sensitive materials. Nahar et al.[30,31] presented highly sensitive humidity sensors using porous Al_2O_3 thin films. Laville and Pellet[38] proposed interdigitated humidity sensors incorporating a plasma-etched polyimide sensing layer. Thin polyimide films exhibit a low humidity sensitivity (4 pF/%RH) at $0\% < RH < 70\%$ and a high sensitivity (75 pF/%RH) at $70\% < RH < 90\%$. It has been reported that thin sensing layer films increase the sensitivity of humidity sensors. To reduce the serious hysteresis problems, Fürjes et al.[36] integrated an internal heater over the moisture sensing layer. However, the hysteresis phenomenon still remains problematic.[32] Porous silicon as a miniaturized humidity sensor material was reported. For example, Björkqvist et al.[35] developed a capacitive humidity sensor using thermally carbonized porous silicon (TC-PS) at room temperature. In their study, long-term stability of porous silicon was improved by thermal oxidation since a stable surface of thermally carbonized PS was formed. In spite of good sensitivity over a wide range of relative humidity and excellent repeatability, the hysteresis above 60% of relative humidity was still observed. Porous SiC was also used for humidity sensing in harsh chemical environments. For instance, Connolly et al.[37] used SiC membrane and Al electrodes rather than Au which was commonly used in conventional humidity sensors such that the fabrication was more clean-room friendly and compatible with CMOS process. Polymer materials were also used for humidity sensing. For example, Matsuguchi et al.[29] developed a capacitive humidity sensor based on a poly(methyl methacrylate) (PMMA) cross-linked with divinylbenzene (DVB). Thanks to the rigid cross-linked structures in the polymer, the irreversible increase in volume of the sensing layers caused by swelling was prevented, which improved the long-term stability of the capacitive humidity sensors.

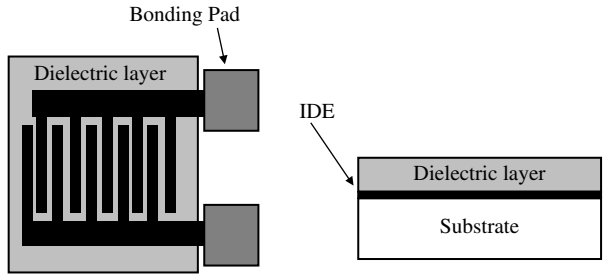

Figure 5. Capacitive humidity sensors with interdigitated electrodes. Typically, capacitive humidity sensors are composed of two interdigitated electrodes (IDE) covered by a dielectric layer, which is sensitive to humidity change.

Typically, ceramics have the advantages of high mechanical strength and the ability to function correctly at high temperatures. Ceramics used in humidity sensing applications include $MgCr_2O_4$, TiO_2 and Al_2O_3. Compared to ceramics, polymers are more readily applied to sensing devices and are more compatible with standard IC fabrication technology. Typical hygroscopic polymers include cellulose acetate, polymethyl methacrylate, polyimide,[39–41] plasmapolymerized hexamethyldisilazane (HMDSN)[42] and polyethersulphone.[40] For example, Gu et al.[41] reported a capacitive humidity sensor integrated with a polysilicon heater using a CMOS process. The humidity sensing material, polyimide, was deposited by a post-processing step after the standard CMOS fabrication. The integrated heater was shown to be able to improve the speed of moisture desorption and eliminate the volatile impurity. A quick response time (10 s) was observed in their study.

Systematic investigations have shown that the ambient humidity has a significant influence on both the electrical and mechanical properties of polyimide.[43] When using a bulk polyimide film as the sensing material, the humidity is generally determined from capacitance measurements and a good linear relationship is obtained between the output signal and the relative humidity.[44,45] A change of 25–28% normalized capacitance has been reported as the RH value is increased from 0–100%.[46] Some modified polyimide films using 3-dimensional micro-structures to enlarge the active surface and to improve the measuring sensitivity have also been reported.[47,48]

REVIEW

Other designs of capacitive humidity sensors were developed in recent years. For example, Chakraborty et al.[49] proposed a moisture sensitive field effect transistor (FET) using $SiO_2/Si_3N_4/Al_2O_3$ gate structures. Harpster et al.[50] developed a passive wireless humidity sensor consisting of an electroplated copper coil for wireless operation and a polyimide film for humidity sensing. A divinyl siloxane benzocyclobutene (BCB) thin film was used as a moisture sensing layer with a sensitivity of 0.1 pF/%RH and a fast response time of 650 ms.[51] Humidity sensors based on nano-structured carbon films produced by supersonic cluster beam deposition were also presented. A sensitivity of 0.1–0.5 pF/%RH in the relative humidity range 10–70% was reported.[52] The nano-structured carbon films were obtained using pure helium gas as the buffer gas in the pulsed microplasma cluster source (PMCS).

Recently, emerging MEMS (Micro-electro-mechanical-systems) technology and micromachining techniques have had a substantial impact on the miniaturization of sensors. These techniques have facilitated the development of new micro-scale sensing instrumentation capable of accessing information in a rapid and accurate fashion. Significantly, the functionality and reliability of these micro sensors can be increased through their integration with mature logic IC (integrated circuit) devices and with other sensors. Many previous studies have reported the development and application of MEMS technologies to the fabrication of micro-scale humidity sensors. For example, Lee et al.[126] developed a novel fabrication process for Pt resistor temperature detectors (RTD) and micro-cantilevers covered with a water-absorbent polyimide layer. These devices were then incorporated in an integrated humidity sensor as a micro temperature sensor and a micro capacitive humidity sensor, respectively (Fig. 6). Integrated micro humidity sensors provide the capacitance measurement required for the instantaneous sensing of humidity. Meanwhile, the

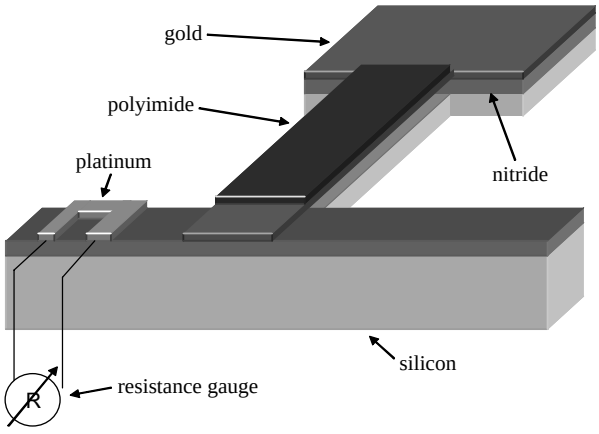

Figure 6. Schematic representation of the integrated humidity sensor and temperature sensor. Absorption of water molecules causes the upper layer of the cantilever to expand, hence inducing a surface tensile stress. As a result, the cantilever bends up, giving rise to a measurable change in the capacitance.[126]

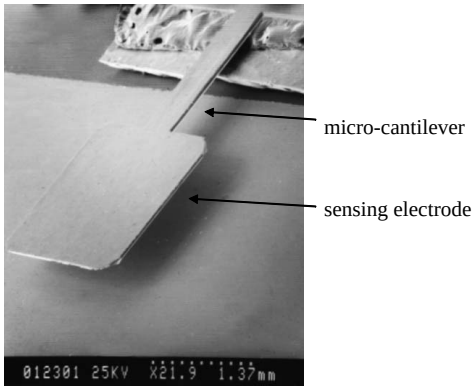

Figure 7. SEM photographic image of the cantilever fabricated for the integrated humidity sensor.[126]

integrated micro temperature sensors permit temperature compensation of the humidity measurement by providing temperature signals to the humidity transducers. Having compensated for temperature drift, the humidity value can be precisely determined from the measured resistance and capacitance signals. The experimental data indicated a high stability ($< \pm 0.8\%$), a low hysteresis (1.9% RH) at high humidity, a high sensitivity (2.0 nF/%RH), and a rapid response time (1.10 sec).

In the capacitance-type integrated humidity sensor, a movable electrode is fabricated by coating a microfabricated cantilever with a material which absorbs water when exposed to humid conditions (Fig. 7). Meanwhile, the second electrode of the capacitor is fixed on a glass substrate. A gold layer is electron-beam evaporated directly on both the moveable cantilever part of the sensor and on the stationary glass substrate. The absorption of water molecules causes the upper layer of the cantilever to expand, and hence induces a surface tensile stress. This causes an upward bending of the suspended structure away from the glass substrate, which changes the capacitance between the two structures.

Previous studies have noted that capacitance-type sensors with a polymer sensing layer are liable to exhibit humidity hysteresis problems. Ideally, a sensor should follow the same capacitance path as the humidity is either increased or decreased. However, in practice, a small degree of hysteresis is exhibited for most humidity sensors, i.e. the capacitance paths for increasing and decreasing humidity differ to some extent. In Lee's investigation, the temperature was maintained at a constant 25 °C while the humidity was increased from 45% RH to 95% RH over a period of 30 minutes and then dehumidified to 45% RH at the same rate. The results revealed that the humidity sensor has a hysteresis of 1.9% RH at high relative humidities (>65% RH) and a value of 0.9% RH at low relative humidities (<65% RH). It is noted that these values are smaller than those reported in previous studies.[27, 80]

In general, capacitive humidity sensors are the most commonly adopted commercially-available humidity sensors. Despite their inherent disadvantages such as hysteresis, slow

Table III. Overview of transduction techniques for capacitive humidity sensors.

Year	Authors	Design	Materials	Output	Remarks	Ref.
1990	Denton et al.	Polyimide sensing layer	Polyimide film	Capacitance	Good linearity	[45]
1991	Boltzhauser et al.	Polyimide sensing layer	Polyimide film	Capacitance	Electrical and mechanical properties of PI	[43]
1995	Story et al.	IDE	Polyimide film	Capacitance	Capacitance and SAW sensing mechanisms	[27]
	Shibata et al.	Converter design	Polyimide film	Capacitance	Capacitance-to-frequency converter	[46]
1997	O'Halloran et al.	IDE	Porous silicon	Capacitance	Use of porous silicon	[33]
1998	Nahar and Khanna	Al-porous Al_2O_3-Au	Porous alumina	Capacitance	Anion incorporation	[30]
1999	Chakraborty et al.	Field effect transistors	Al_2O_3 film	Capacitance	$SiO_2/Si_3N_4/Al_2O_3$ gate structure	[49]
2000	Narhar	Al-porous Al_2O_3-Au	Porous alumina	Capacitance	Pore-widening model incorporation	[31]
	Kang and Wise	Integrated Poly-Si heaters	Polyimide film	Capacitance	Easy to be reset during self-tests	[39]
2001	Dokmeci and Najafi	Polyimide sensing layer	Polyimide film	Capacitance	Good linearity	[44]
2002	Laville and Pellet	Etched sensing layer	Polyimide film	Capacitance	Investigation of materials and thicknesses	[38]
	Yang et al.	Au-polyimide-Au	Polyimide film	Capacitance	Humidity admittance square holes in sensing films	[48]
	Harpster et al.	Remote antenna	Polyimide film	Capacitance	Wireless operation	[50]
	Harrey et al.	Parallel-plate electrodes	Polyimide and PES films	Capacitance	Offset lithographic printing process	[40]
2003	Das et al.	IDE, signal compensation	Porous silicon	Capacitance	Good linearity at high RH range	[34]
	Fürjes et al.	IDE, internal heaters	Porous silicon	Capacitance	Refreshing thermal cycles	[36]
	Laconte et al.	3-layer patterned sensing film	Polyimide film	Capacitance	High sensitivity output	[47]
	Tételin et al.	Parallel-plate electrodes	BCB thin film	Capacitance	Rapid time response	[51]
	Kraus et al.	Plasmapolymerization	HMDSN	Capacitance	Application of HMDSN	[42]
	Lee and Lee	Movable electrodes	Polyimide	Capacitance	Temperature sensors for signal drift compensation	[126]
2004	Björkqvist et al.	Thermally carbonized PS	Porous silicon	Capacitance	Good long-term stability	[35]
	Connolly et al.	Al electrodes	Porous SiC	Capacitance	Suitable for harsh environments	[37]
	Gu et al.	Post-processed polyimide	Polyimide film	Capacitance	CMOS fabrication process	[41]
	Dabhade et al.	IDE	PMMA	Capacitance	Plasma-treated polymer	[28]
	Matsuguchi et al.	Cross-linked structure	PMMA	Capacitance	Improvement of long-term stability	[29]
	Bruzzi et al.	Nano-structured carbon films	ns-C films	Capacitance	Supersonic cluster beam deposition	[52]

response time, low output signals (pF) and temperature-dependency, they continue to be the subject of intensive development efforts due to their high sensitivity and low fabrication costs. Table III summarizes the design and materials used for various capacitive humidity sensing systems.

5. RESISTIVE HUMIDITY SENSORS

The transduction mechanism of resistive humidity sensors involves the changes in conductivity caused by the adsorption of water vapor. Typically, sensors of this type utilize three major categories of materials: (1) ceramics, (2) polymers and (3) electrolytes. The basic configuration of these sensors resembles that of capacitive humidity sensors other than that the dielectric layers are replaced by conductivity-sensitive layers.

Many previous studies utilized metal oxides with a hubnerite and spinel structure, such as WO_3, $PbWO_4$, MoO_3, $ZrTiO_3$, $LaFeO_3$, $ZnWoO_4$, WO_3-Y_2O_3 composite, ZnO-Y_2O_3 composite, K_2O doped $Ba_{0.5}Sr_{0.5}TiO_3$, $Sm_{1-x}Sr_xCrO_3$ ($0 < x < 1$), $La_{1-x}Sr_xFeO_3$ ($0.1 < x < 0.4$), $MMoO_4$ (M = Ni, Cu, Pb), $Mg_{0.5}Cu_{0.5}Fe_{2-x}M_xO_4$ ($x = 0$ or 0.2, M = La or Ga), Li-Fe_2O_3, $MnWO_4$, $NiWO_4$, $CoWO_4$, $ZnCr_2O_4$, $MgCrO_4$, TiO_2, $MgAl_2O_4$, hematite, ZnO, Al_2O_3, etc.[53–69] For example, Qu and Meyer[53,70] presented a thick-film porous $MnWO_4$ ceramic layer sandwiched by interdigitated metal films. Sundaram and Nagaraja[56] used $PbWO_4$ and WO_3 composites for humidity sensing. High sensitivity and quick response were observed in their study. Composites of $MMoO_4$ (M = Ni, Cu, Pb) and MoO_3 were also reported for their good humidity sensing characteristics.[67] A ceramic thick-film humidity sensor with good humidity sensitivity was demonstrated using an emulsion of titania powders by a low-speed spin-coating technique.[60] Although possessing a humidity dependency, the resistance of these sensors generally decreases with ambient temperature. Temperature effects can generate a signal drift, which represents a serious problem for this type of humidity sensor.

Ying et al.[71] presented a humidity sensor based on TiO_2–K_2O–$LiZnVO_4$ ceramic thin films prepared using the sol–gel technique. Excellent humidity sensitive properties were attained over the range of 10–90% RH. Sol–gel $BaTiO_3$,[72] sol–gel silica films synthesized by block copolymers,[73] sol–gel strontium-doped lead-zirconium-titanate ($PS_xZ_{0.3}T_{0.7}O_3$, $x = 0.1$–0.5)[74] and sol–gel chromium titanate oxide ($Cr_{2-x}Ti_xO_3$, $x = 0.05$–0.4)[75] were also used as moisture sensing layers. It was found that

Table IV. Overview of transduction techniques for resistive humidity sensors.

Year	Authors	Design	Materials	Output	Remarks	Ref.
1989	Yeh and Tseng	Ion doping	K_2O doped $Ba_{0.5}Sr_{0.5}TiO_3$	Conductance	Good linearity	[64]
1991	Lu et al.	Ceramic application	$La_{1-x}Sr_xFeO_3$ $(0.1 \leq x \leq 0.4)$	Resistance	Investigation of ceramic materials	[66]
1995	Sakai et al.	Crosslinked and quaternized	Polymers	Impedance	Durable at high RH range	[84]
1996	Sakai et al.	Graft polymerization	Polymers	Impedance	Modified by cross-linking	[85]
1997	Qu and Meyer	Thick-film technology	Porous $MnWO_4$	Resistance	Temperature compensation	[53]
	Barkauskas	Composite materials	Polyvinylalcohol and graphitized carbon black disperse phase	Resistance	Study of materials	[78]
	Wang et al.	Polymer materials	PVA, TA and Nafion	Impedance	Study of materials	[79]
	Feng et al.	Sol–gel applications	Sol–gel SiO_2/Nafion	Impedance	Study of materials	[54]
	Golonka et al.	Thick film technology	ZCT ceramics	Impedance	Study of materials	[105]
1998	Sakai et al.	Polymer materials	Polymers with pyridinium groups	Impedance	Study of materials	[83]
1999	Chou et al.	Porous ceramics	Ceramic fiber, kaolin and CMC	Resistance	Study of materials	[55]
2000	Qu et al.	Thin-film technology	$MnWO_4$	Resistance	Fast time response	[70]
	Ying et al.	Ceramic application	TiO_2-K_2O-$LiZnVO_4$	Impedance	Sol–gel processed	[71]
	Sakai et al.	Cross-linking and quaternization	PCMS	Impedance	Study of materials	[86]
2001	Su et al.	Thick-film technology	Poly-AMPS modified with TEOS	Impedance	Low hysteresis and high linearity	[80]
	Lee et al.	Epoxy resin formation	GTMAC	Impedance	Study of materials	[93]
2002	Raj et al.	Composite materials	$ZnMoO_4$ and ZnO	Resistance	Study of materials	[61, 62]
	Arshak et al.	Composite materials	MnO, ZnO and Fe_2O_3	Resistance	High reliability	[76]
	Wang et al.	Composite materials	Nanocrystal $BaTiO_3$-RMX	Resistance	Study of materials	[82]
	Li and Yang	Salt doping	Poly(2-propyn-2-furoate)	Impedance	Study of materials	[91]
	Gong et al.	Cross-linked poly-electrolyte	Mutually reactive copolymers	Impedance	Study of materials	[87]
	Gong et al.	Electrolyte application	Cross-linked copolymers	Resistance	Study of materials	[92]
	Son et al.	Phosphonium salt-containing	VTBPC	Resistance	Study of materials	[88]
	Li and Yang	Bilayer thin film	Polymers	Impedance	Study of materials	[89]
	Suri et al.	Nano-composite materials	Fe_2O_3-polypyrrole	Impedance	Study of materials	[95]
	Yang et al.	IDE	Polymer electrolytes	Impedance	Study of materials	[97]
	Park et al.	Mutually reactive copolymers	Gel polyelectrolyte	Impedance	Study of materials	[96]
	Varghese et al.	Al_2O_3-Pt	Al_2O_3 thin film	Impedance	Investigation of pore size and uniformity of sensing layers	[77]
2003	Pokhrel et al.	Metal oxide application	WO_3 and MoO_3	Resistance	Non-linear relationship at high RH range	[57]
	Cosentino et al.	Ceramic application	$ZrTiO_3$	Impedance	Non-linear relationship at high RH range	[58]
	Neri et al.	Metal doping	Fe_2O_3 doped Li or Au	Resistance	Investigations of metal dopings	[69]
	Yuk et al.	Al_2O_3-$BaTiO_3$-Au	$BaTiO_3$	Impedance	Sol–gel process	[72]
	Wang et al.	Composite materials	Nanocrystalline $BaTiO_3$-PSS	Resistance	Material study	[81]
	Lee et al.	Electrolyte application	Cross-linked polyelectrolytes	Resistance	Material study	[103]
	Lee et al.	Electrolyte application	Cross-linked polyelectrolytes	Impedance	Materials study	[94]
	Bearzotti et al.	Block copolymers synthesis	Mesoporous SiO_2 thin films	Current	Material study	[98]
	Ingram et al.	Laser carbonized polyimide substrate	HMPTAC and PEO-$LiClO_4$	Impedance	Material study	[99]
2004	Sundaram et al.	Metal oxide application	WO_3 and $PbWO_4$	Resistance	Non-linear relationship at high RH range	[56]
	Sundaram et al.	Composite materials	WO_3-Y_2O_3 composite	Resistance	Solid state electrical conductivity measurement	[63]
	Sundaram et al.	Ceramic application	$MMoO_4$ (M = Ni, Cu, Pb)	Resistance	Solid state electrical conductivity measurement	[67]
	Sundaram et al.	Ceramic application	$Sm_{1-x}Sr_xCrO_3$ $(0 \leq x \leq 1)$	Impedance	Microwave assisted synthesis	[65]

continue

Table IV. Continued.

Year	Authors	Design	Materials	Output	Remarks	Ref.
	Wang et al.	Ceramic application	$LaFeO_3$	Impedance	Non-linear relationship at high RH range	[59]
	Wang et al.	Composite materials	BCN18	Conductivity	Proton conducting perovskite oxides	[101]
	Faia et al.	Thick film technology	TiO_2	Resistance	A slow spinning process	[60]
	Rezlescu et al.	Ion doping	$Mg_{0.5}Cu_{0.5}Fe_{2-x}M_xO_4$ ($x = 0$ or 0.2, M = La or Ga)	Resistance	Investigations of ion dopings	[68]
	Bearzotti et al.	Meso-structured films	SiO_2 films	Current	Sol–gel process	[73]
	Fratoddi et al.	HCl, $SnCl_2$ and I_2 doping	Poly-acetylenes	Current	Material study	[90]
	Li et al.	*In-situ* synthesized inorganic/organic nanocomposites	NaPSS-ZnO composite	Impedance	Material study	[100]
	Ansari et al.	Sr-doping nano-particles	$PS_xZ_{0.3}T_{0.7}O_3$ ($x = 0.1$–0.5)	Resistance	Investigation of Sr doping level	[74]
	Litovchenko et al.	PS-based MIS-structures	Cu/Pd-porous silicon-silicon	Band gap	Current-voltage characteristics	[104]
	Su et al.	Nano-sized composites	SiO_2-poly(AMPS) composites	Impedance	Material study	[102]
	Neri et al.	Low temperature sol–gel synthesis	$Cr_{2-x}Ti_xO_3$	Resistance	Material study	[75]

the control of dimension, shape and distribution of pores in these materials was crucial for the fabrication of the mesostructured thin-film humidity sensors. Using di-block, tri-block or star-block, 2-D hexagonal mesoporous phases in silica were formed and good performances in humidity sensing were exhibited.[73] Neri et al.[75] reported the low temperature sol–gel synthesis of chromium titanate oxide (CTO) for the sensing material of resistive humidity sensors. The influence of the doping level of the base material on the humidity sensing performance was also explored. Using sol–gel technique from alkaoxides, Ansari et al.[74] prepared $PS_xZ_{0.3}T_{0.7}O_3$ ($x = 0.1$–0.5) nano-particles calcined at different temperatures from 500 to 700 °C. While increasing Sr doping level (0.1 M–0.5 M), the band gap in current-voltage (I-V) characteristics was reduced. 0.5 M Sr doping concentration was found to be the optimum condition suitable for relative humidity sensing in the range of 20–100% RH which gave rise to high sensitivity and low barrier height. However, the problem of temperature drift was still evident. Arshak et al.[76] developed a thick-film resistive humidity sensor using a combination of MnO, ZnO and Fe_2O_3. It was shown that this sensor yielded a high linearity, lower hysteresis (0.35% RH) and a fast response time (11–28 sec). Varghese et al.[77] reported the effect of pore size and uniformity on sensing performance for nanoporous Al_2O_3 films. It was reported that the response of the material to humidity was a strong function of pore size and operating frequency. A well-behaved change in impedance more than three orders of magnitude variation over 20% to 90% RH was reported for nanoporous Al_2O_3 films with an average pore size of 13.6 nm.

Due to their ease of fabrication, low cost, and adjustable properties, polymer materials have significant potential for application to humidity sensors.[77–90] Barkauskas[78] developed a resistive humidity sensor using a sensing film prepared from PVA (polyvinyl alcohol) and graphitized carbon black disperse phase. The experimental data revealed a sensitivity of 8 ohm/%RH at room temperature and 5 ohm/%RH at 100 °C. However, the response time of this sensor is 45 sec, which is slower than that of the ceramic-type sensor. Wang et al.[79] demonstrated a humidity sensor using Nafion in different ionic forms (H^+, Li^+ and Na^+) prepared using casting techniques. It was shown that the content of the cation in the Nafion has a significant influence on the sensing properties of the film. Su et al.[80] presented a resistive humidity sensor fabricated by thick film techniques using poly (2-acrylamido-2-methylpropane sulfonate) (poly-AMPS) modified with tetraethyl orthosilicate (TEOS) as the sensing material. This sensor was simple to fabricate and exhibited a reduced degree of hysteresis (<2%), good linearity ($R^2 = 0.9989$) at humidity levels in the range 30–90% RH, long-term stability and satisfactory resistance to high humidity atmospheres (e.g. 95% RH). Fratoddi et al.[90] investigated the resistive-type humidity sensors based two poly(monosubstituted)acetylenes, namely poly(*N*,*N*-dimethylpropargylamine) (Pd-PDMPA) and poly(propargylalcohol) (PPOH). These sensors exhibited detectable responses to relative humidity as low as 2% and a variation of five orders of magnitude in the relative humidity range 0–90%.

Ceramic/polymer composite thin films have also been used to optimize the performance of resistive humidity sensors.[54, 55, 81–86, 91–102] For example, Feng et al.[54] prepared SiO_2/Nafion composite thin films using casting and dip-coating methods. The performance of Nafion film sensors is determined by the migration of hydrogen ions through the film. At high RH, the total impedance includes the contribution of a faradic impedance at the electrode-film interface. The use of a SiO_2/Nafion composite film permits a significant reduction in the faradic impedance, hence yielding an improved linearity of the sensor response. Chou et al.[55] investigated a humidity sensor with porous ceramics fabricated from ceramic fiber, kaolin and sodium salt of carboxylmethyl cellulose (CMC). The conductivity was

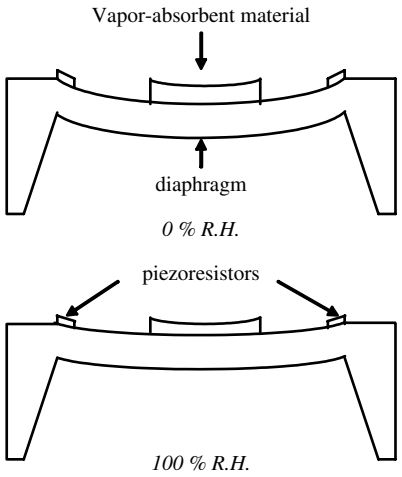

Figure 8. General layouts of piezoresistive humidity sensors. The membrane-type device uses piezoresistors placed on top of the diaphragm. As the humidity increases, the resulting humidity-dependent volume change of the polyimide layer prompts a deformation of the polyimide-bridge substrate bimorph and therefore leads to a bending of the plate, which is then transformed into an output voltage by an integrated piezoresistive bridge.[107]

shown to change by 4–5 orders of magnitude when the RH varied from 10 to 90%. Furthermore, the response time was reported to be 5–8 min for RH values of 10 to 90%. Wang et al.[81, 82] reported a humidity sensing composite material composed of nano-crystalline $BaTiO_3$ and polymer polystyrene sulfonic sodium (PSS). $BaTiO_3$/PSS humidity sensors possess good sensitivity and linearity characteristics at RH ranges of 33–98%, and exhibit a maximum humidity hysteresis of 8% RH. Additionally, the response and recovery times of these sensors are 50 and 120 sec, respectively. This performance is clearly a significant improvement over that of previous polymer sensing materials. Su and Tsai[102] used a composite material of nano-sized SiO_2 and poly(2-Acrylamido-2-methylpropane sulfonate) (poly(AMPS)) to fabricate a resistive humidity sensor. The sensor showed a negligible hysteresis and fast response upon humidification and dehumidification. The applications of nano-sized materials significantly improved the hysteresis.

Sakai et al.[83–86] developed resistive-type humidity sensors using humidity-sensitive and water-resistive polymetric materials such as quaternized vinylpyridine and styrene copolymers, partially quaternized polyvinylpyridine, polytetrafluoroethylene grafted with quaternized polyvinylpyridine, polyvinylpyridine crosslinked with dibromobutane, poly(2-hydroxy-3-methacryloxypropyl-trimethyl ammonium chloride) cross-linked with hexamethylene diisocyanate, simultaneously crosslinked and quaternized polychloromethyl styrene (PCMS). These sensors demonstrated excellent water resistivity and high sensitivity to humidity. Gong et al.[92] proposed humidity sensors using cross-linked polyelectrolyte prepared from mutually reactive copolymers containing phosphonium salt. These sensors showed average resistances of 725, 43 and 3.1 kΩ at 30, 60 and 90% RH respectively. They were also found to be comparatively resistant to water. Lee et al.[93, 94, 103] proposed two types of resistive humidity sensors using epoxy resin containing quaternary ammonium salts and polyelectrolytes based on new-type mutually cross-linkable copolymers. The impedance of the latter type varies from 755 to 2.52 kΩ in the humidity range of 30% to 90% RH. Cross-linking techniques provide an efficient means of improving the water durability and of providing a long-term stability (300 days). Furthermore, these devices have a rapid response time, typically less than 75 sec when the humidity is changed abruptly from 33 to 94% RH. Using *in-situ* synthesized inorganic/organic nanocomposites of sodium polystyrenesulfonate (NaPSS) and ZnO, Li et al.[100] developed thin film humidity sensors with four-orders of magnitude sensitivity over 11–97% RH, small hysteresis (less than 2% RH) and quick response time (absorption: 2 s, desorption: 2 s). A conductimetric humidity sensor based on proton conducting perovskite oxide ($Ba_3Ca_{1.18}Nb_{1.82}O_{9-\delta}$-BCN18) was also reported.[101] Dense and porous samples of an oxygen deficient perovskite oxide were fabricated by sintering powder compacts of calcined powders. It was found that porous material had 5–6 times faster time response than that for the dense material. The relatively rapid response of the porous material suggests a promising conductimetric humidity sensor based on porous BCN18 as a good sensing material. Porous silicon (PS)-based metal-insulator-semiconductor (MIS)-structures have been used as moisture sensing materials. The mechanism of humidity sensing has been studied.[104] The current-voltage (I-V) characteristics of these materials could be used for humidity sensing.

Typically, resistive humidity sensors offer the advantages of simple electrical circuits, high sensitivity and good linearity. However, humidity hysteresis is a problem

Table V. Overview of transduction techniques for piezoresistive humidity sensors.

Year	Authors	Design	Materials	Output	Remarks	Ref.
1994	Sager et al.	Enlargement of sensing surface	Polyimide	Voltage	Experiments and modeling	[108]
1995	Schroth et al.	Resonant polyimide-based	Polyimide	Voltage	Volume expansion caused by water absorption	[106]
	Sager et al.	Piezoresistive sensors	Polyimide	Voltage	Investigation of failure source	[109]
1996	Sager et al.	Humidity-dependent mechanical properties	Polyimide	Voltage	Piezoresistive humidity sensors	[110]
1998	Buchhold et al.	Thin-film technology	Polyimide	Voltage	Dependent of diaphragm shapes	[107]

Table VI. Overview of transduction techniques for magnetoelastic humidity sensors.

Year	Authors	Design	Materials	Output	Remarks	Ref.
2000	Grimes et al.	Remote query	TiO_2 thin film	Resonant frequency	Nanoporous sensing layer	[124]
	Barandiaran et al.	Remote query	Al_2O_3 thin film	Resonant frequency	Sensing of pressure, fluid-flow velocity and humidity	[114]
2001	Schmidt et al.	Thermal evaporation of Al and Ag	Al, Ag thin film	Resonant frequency	Investigation of thin-film elastic moduli	[119]

when these sensors are employed on a periodic rather than continuous basis. Furthermore, the sensing materials have a relatively slow response and the long-term stability of the device can only be guaranteed by a continuous operation and by attentive maintenance. Although humidity sensitive materials are still under development, commercially-available resistive humidity sensors are generally made of polymer or porous ceramics. Thick film technology is desirable for the mass production of resistive humidity sensors on account of its cost efficiency, robustness and flexibility in device design.[105] Table IV summarizes the design and materials used for various resistive humidity sensing systems.

6. PIEZORESISTIVE HUMIDITY SENSORS

Piezoresistive materials have found widespread application in human-made sensors. Nowadays, transduction from air humidity via mechanical domain is a mature sensing technique. Typically, piezoresistive humidity sensors utilize a suspended structure coated with a water-absorbent layer (Fig. 8). Polymer-based films have 2–6% water absorption, which results in a volume expansion ratio of approximately 5.5×10^{-5}/%RH.[106] Piezoresistors are used to detect the bending of this structure prompted by humidity changes. Buchhold et al.[107] adopted the use of piezoresistors located on top of a diaphragm coated with a layer of polyimide. As the humidity increased, the humidity-dependent volume change of the polyimide layer prompted a deformation of the polyimide-bridge substrate bimorph and, therefore caused a bending of the plate, which was then transformed into an output voltage by an integrated piezoresistive bridge. It has been shown that the sensitivity of piezoresistive humidity sensors with resistors located at the periphery of the diaphragm does not depend significantly on the shape of the diaphragm. Hence, the specification of the diaphragm shape can be based solely on technological considerations.

Sager et al.[108–110] investigated the humidity-dependent mechanical properties of polyimide films and their application to piezoresistive humidity sensors. The coefficient of humidity expansion (CHE) was shown to be approximately 60 to 80 ppm/%RH at different polyimide curing temperatures. The expansion can be used to create piezoresistive humidity sensors operating in a similar fashion to bimetal elements influenced by ambient temperature.

The major difficulty in designing piezoresistive humidity sensors lies in providing an adequate thermal coupling to ensure a precise temperature control. Additionally, as in other sensor types, temperature drift is a significant problem for piezoresistive humidity sensors. Table V summarizes the design and materials for various piezoresistive humidity sensors.

7. MAGNETOELASTIC HUMIDITY SENSORS

The variation of the magnetoelastic resonance frequency could be used to monitor environmental parameters for remote query applications.[111–113] It also could be used for relative humidity sensing. The transduction mechanism of magnetoelastic humidity sensors is based on the resonant frequency shift of the magnetic flux emitted from the sensors in response to a time varying magnitude field. For example, a remote query humidity sensor made by coating the magnetoelastic thick film with a thin layer of sol–gel deposited Al_2O_3 was reported by Grimes and Kouzoudis.[114] In addition to humidity, other environmental parameters including temperature,[115] DC magnetic field,[116] surface stress,[111] tension,[117] liquid density and viscosity,[113, 118] displacement,[112] atmospheric pressure, thin-film elastic modulus,[119] level of liquids,[112] mass loading[115] and fluid-flow velocity[114] could be monitored by the magnetoelastic sensors. Remote query measurement of chemicals could also be achieved using the type of magnetoelastic sensors, including glucose,[115] NH_3,[120] CO_2,[121] and pH.[122, 123]

The operation principle of the magnetoelastic humidity sensors could be described as follows. The resonant frequency of the magnetoelastic sensor changes in response to mass loading within moisture sensing layers while relative humidity changes. Change of the mass results in a resonant frequency shift, which could be represented by the following formula[113]

$$\Delta f = -\frac{f}{2}\frac{\Delta m}{M} \tag{6}$$

Thus small changes in mass can be detected by monitoring the shift in the resonance frequency of the magnetoelastic sensor. The magnetoelastic sensors with a layer of moisture absorbing and desorbing material could be used for remote query measurement of humidity. The humidity-sensitive thin films including Al_2O_3,[114] porous TiO_2,[124] and

$Fe_{73.5}Cu_1Nb_3Si_{13.5}B_9$[125] were reported in previous studies. Table VI summarizes the design and materials for various magnetoelastic humidity sensors.

8. CONCLUSIONS

Humidity sensors are widely applied in the environmental monitoring, electronics, agricultural, and bio-medical fields. For many applications, not only humidity, but also temperature is an important factor. Therefore, there exists a strong demand for simply-fabricated integrated humidity and temperature sensors in many fields.

Miniaturization technology has facilitated the development of micro humidity sensors, which generally adopt vapor-absorbent films as their sensing materials.[27, 31, 70, 76, 80] The electric/mechanical properties of these films change as the relative humidity changes, and these changes allow the precise value of the relative humidity to be determined. However, it still remains challenging to develop a sensor which provides a complete set of favorable characteristics, e.g. good linearity, high sensitivity, low hysteresis and rapid response time.

This review paper has briefly introduced the optical-, gravimetric-, capacitive-, resistive-, piezoresistive- and integrated-types of humidity sensors. New fabrication processes are under continuous development in the commercial and research fields. In today's market, there exists an increasing requirement for low cost, highly reliable functional humidity sensors. The integrated sensor discussed in this review paper represents an appropriate choice to satisfy this demand.

GLOSSARY

Dew point The temperature at which the air would have to cool (at constant pressure and constant water vapor content) in order to reach saturation. Condensation of water vapor commences when the temperature of the air is lowered to the dew point.

Dry-bulb temperature The temperature of the air-water vapor flow measured by the dry-bulb thermometer.

Helmholtz coils A pair of circular coils separated by a distance equal to the coil radius. This spacing optimizes the homogeneity of the magnetic field that is produced by equal current flowing through each coil. Although a Helmholtz pair could form the basis of a magnet, in practical applications, more complex coil arrangements are needed in order to achieve the exceptionally high degree of field homogeneity required for this application.

Hysteresis A retardation of the recovery when the physical quantity of a body is changed.

Magnetoelastic The transduction mechanism of magnetoelastic sensors is based on the resonant frequency shift of the magnetic flux emitted from the sensors in response to a time varying magnitude field.

MEMS Micro-Electro-Mechanical-System (MEMS) is the integration of mechanical elements, sensors, actuators, and micro-electronics on a common silicon substrate through microfabrication technology. While the electronics are fabricated using integrated circuit (IC) process sequences (e.g., CMOS or bipolar processes), the micromechanical components are fabricated using compatible "micromachining" processes that selectively etch away parts of the silicon wafer or add new structural layers to form the suspended or movable mechanical and electromechanical devices.

Metal-oxide-semiconductor field-effect-transistor (MOSFET) A FET with an oxide coating between the gate and the channel is called a MOSFET. Current flows in the channel between a source and a drain. Channel is created by applying adequate potential to the gate contact and inverting semiconductor surface underneath the gate.

Metal-insulator-semiconductor field-effect-transistor (MISFET) The MISFET is a certain type of field effect transistor which is especially well suited to the compound semiconductor materials; more general term than Metal-Oxide-Semiconductor FET, but describing the same device structure.

Moisture The amount of water absorbed by a solid or a liquid or chemically bound to a liquid.

Piezoresistor A resistor whose resistance undergoes a fractional change in bulk resistivity as a result of small mechanical stresses applied to the material.

Quartz crystal microbalance A highly sensitive mass balance, capable of sensing changes of mass within the nanogram range. The operation of the microbalance is based on the resonance behavior of the crystal, i.e. the resonant frequency depends on the total oscillating mass.

Refractive index Ratio of the speed of an electromagnetic wave in a vacuum compared to its speed in a matter.

Relative humidity Ratio of the mass of water vapor in a unit volume compared to the mass of water vapor which that volume could hold if the vapor were saturated at the mixture temperature.

Sol–gel techniques The sol–gel process is a versatile solution process for making ceramic and glass materials. In general, the sol–gel process involves the transition of a system from a liquid "sol" (mostly colloidal) into a solid "gel" phase. The starting materials used in the preparation of the "sol" are usually inorganic metal salts or metal organic compounds such as metal alkoxides. In a typical sol–gel process, the precursor is subjected to a series of hydrolysis and polymeration reactions to form a colloidal suspension, or a "sol." Further processing of the "sol" enables one to make ceramic materials in different forms. Thin films can be produced on a piece of substrate by spin-coating or dip-coating.

Surface acoustic wave (SAW) Elastic waves traveling on the surface of a piezoelectric material. This phenomenon

can be exploited in acoustic sensors to detect physical, chemical or biological quantities while operating at frequencies in the megahertz to gigahertz range.

Temperature coefficient of resistance Ratio of the resistance change per degree of temperature compared to the resistance value at 0 °C.

Wet-bulb temperature The temperature of the air-water vapor flow measured by the wet-bulb thermometer. If the air-water vapor flow is not saturated, then water will evaporate from the wick on the wet bulb, which then causes a drop in the temperature of the wet-bulb thermometer due to the water evaporation from the wick on the wet bulb.

References and Notes

1. G. J. W. Visscher, *Meas. Sci. Technol.* 6, 1451 (**1995**).
2. J. R. Simões-Moreira, *Meas. Sci. Technol.* 10, 302 (**1999**).
3. Z. M. Rittersma, *Sens. Actuators A* 96, 196 (**2002**).
4. A. Kharaz and B. E. Jones, *Sens. Actuators A* 46, 491 (**1995**).
5. C. Bariáin, I. R. Matías, F. J. Arregui, and M. López-Amo, *Sens. Actuators B* 69, 127 (**2000**).
6. B. Schirmer, H. Venzke, A. Melling, C. S. Edwards, G. P. Barwood, P. Gill, M. Stevens, R. Benyon, and P. Mackrodt, *Meas. Sci. Technol.* 11, 382 (**2000**).
7. P. R. Somani, A. K. Viswanath, R. C. Aiyer, and S. Radhakrishnan, *Sens. Actuators B* 80, 141 (**2001**).
8. N. T. T. Ha, D. K. An, P. V. Phong, P. T. M. Hoa, and L. H. Mai, *Sens. Actuators B* 66, 200 (**2000**).
9. B. D. Gupta and Ratnanjali, *Sens. Actuators B* 80, 132 (**2001**).
10. S. K. Shukla, G. K. Parashar, A. P. Mishra, Puneet Misra, B. C. Yadav, R. K. Shukla, L. M. Bali, and G. C. Dubey, *Sens. Actuators B* 98, 5 (**2004**).
11. M. Bedoya, G. Orellana, and M. C. Moreno-Bondi, *Helvetica Cheimica Acta* 84, 2628 (**2001**).
12. M. M. F. Choi and S. Shuang, *The Analyst* 125, 301 (**2000**).
13. B. Sorli, F. Pascal-Delannoy, A. Giani, A. Foucaran, and A. Boyer, *Sens. Actuators A* 100, 24 (**2002**).
14. S. M. Drew, J. E. Mann, B. J. Marquardt, and K. R. Mann, *Sens. Actuators B* 97, 307 (**2004**).
15. A. Bozóki, M. Szakáll, Á. Mohácsi, G. Szabó, and Z. Bor, *Sens. Actuators B* 91, 219 (**2003**).
16. H. Wohltjen, *Sens. Actuators* 5, 307 (**1984**).
17. K. A. Vetelino, P. R. Story, R. D. Mileham, and D. W. Galipeau, *Sens. Actuators B* 35, 91 (**1996**).
18. C. Caliendo, E. Verona, and V. I. Anisimkin, *Smart Mater. Struct.* 6, 707 (**1997**).
19. D. W. Galipeau, P. R. Story, K. A. Vetelino, and R. D. Mileham, *Smart Mater. Struct.* 6, 658 (**1997**).
20. E. R. Braga, A. Y. Nakano, and M. P. Cunha, *Proc. SBMO/IEEE MTT-S IMOC '99* 342 (**1999**).
21. P. Bruno, G. Cicala, F. Corsi, A. Dragone, and A. M. Losacco, *Sens. Actuators B* 100, 126 (**2004**).
22. M. K. Jain, S. Schmidt, K. G. Ong, C. Mungle, and C. A. Grimes, *Smart Mater. Struct.* 9, 502 (**2000**).
23. M. Penza and G. Cassano, *Sens. Actuators B* 68, 300 (**2000**).
24. J. Reibel, U. Stahl, T. Wessa, and M. Rapp, *Sens. Actuators B* 65, 173 (**2000**).
25. E. Radeva, V. Georgiev, L. Spassov, N. Koprinarov, and St. Kanev, *Sens. Actuators B* 42, 11 (**1997**).
26. A. Glück, W. Halder, G. Lindner, H. Müller, and P. Weindler, *Sens. Actuators B* 19, 554 (**1994**).
27. P. R. Story, D. W. Galipeau, and R. D. Mileham, *Sens. Actuators B* 24, 681 (**1995**).
28. R. V. Dabhade, D. S. Bodas, and S. A. Gangal, *Sens. Actuators B* 98, 37 (**2004**).
29. M. Matsuguchi, M. Yoshida, T. Kuroiwa, and T. Ogura, *Sens. Actuators B* 102, 97 (**2004**).
30. R. K. Nahar and V. K. Khanna, *Sens. Actuators B* 46, 35 (**1998**).
31. R. K. Nahar, *Sens. Actuators B* 63, 49 (**2000**).
32. R. C. Erson, R. S. Muller, and C. W. Tobias, *Sens. Actuators A* 23, 835 (**1990**).
33. G. M. O'Halloran, P. M. Sarro, J. Groeneweg, P. J. Trimp, and P. J. French, *Proc. Transducers '97* 1, 563 (**1997**).
34. J. Das, S. Dey, S. M. Hossain, Z. M. C. Rittersma, and H. Saha, *IEEE Sens. J.* 3, 414 (**2003**).
35. M. Björkqvist, J. Salonen, J. Paski, and E. Laine, *Sens. Actuators A* 112, 244 (**2004**).
36. P. Fürjes, A. Kovács, Cs. Dücső, M. Ádám, B. Müller, and U. Mescheder, *Sens. Actuators B* 95, 140 (**2003**).
37. E. J. Connolly, H. T. M. Pham, J. Groeneweg, P. M. Sarro, and P. J. French, *Sens. Actuators B* 100, 216 (**2004**).
38. C. Laville and C. Pellet, *IEEE Transactions on Biomedical Engineering* 49, 1162 (**2002**).
39. U. Kang and K. D. Wise, *IEEE Trans. Electron Devices* 47, 702 (**2000**).
40. P. M. Harrey, B. J. Ramsey, P. S. A. Evans, and D. J. Harrison, *Sens. Actuators B* 87, 226 (**2002**).
41. L. Gu, Q. A. Huang, and M. Qin, *Sens. Actuators B* 99, 491 (**2004**).
42. F. Kraus, S. Cruz, and J. Müller, *Sens. Actuators B* 88, 300 (**2003**).
43. T. Boltshauser, L. Chandran, H. Baltes, F. Bose, and D. Steiner, *Sens. Actuators B* 5, 161 (**1991**).
44. M. Dokmeci and K. Najafi, *J. Microelectromechanical Systems* 10, 197 (**2001**).
45. D. D. Denton, C. N. Ho, and S. G. He, *Proc. IEEE Trans. Instrum. Measurement* 39, 508 (**1990**).
46. H. Shibata, M. Ito, M. Asakura, and K. Watanabe, *Proc. IEEE Instrum. Measurement Technology Conference* 100 (**1995**).
47. J. Laconte, V. Wilmart, D. Flandre, and J. P. Raskin, *Proc. IEEE Sens.* 1, 372 (**2003**).
48. Y. L. Yang, L. H. Lo, I. Y. Huang, H. J. H. Chen, W. S. Huang, and S. R. S. Huang, *Proc. IEEE Sens.* 1, 511 (**2002**).
49. S. Chakraborty, K. Nemoto, K. Hara, and P. T. Lai, *Smart Mater. Struct.* 8, 274 (**1999**).
50. T. J. Harpster, B. Stark, and K. Najafi, *Sens. Actuators A* 95, 100 (**2002**).
51. A. Tételin, C. Pellet, C. Laville, and G. N'Kaoua, *Sens. Actuators B* 91, 211 (**2003**).
52. M. Bruzzi, S. Miglio, M. Scaringella, G. Bongiorno, P. Piseri, A. Podesta, and P. Milani, *Sens. Actuators B* 100, 173 (**2004**).
53. W. Qu and J. U. Meyer, *Meas. Sci. Technol.* 8, 593 (**1997**).
54. C. D. Feng, S. L. Sun, H. Wang, C. U. Segre, and J. R. Stetter, *Sens. Actuators B* 40, 217 (**1997**).
55. K. S. Chou, T. K. Lee, and F. J. Liu, *Sens. Actuators B* 56, 106 (**1999**).
56. R. Sundaram and K. S. Nagaraja, *Materials Research Bulletin* 39, 581 (**2004**).
57. S. Pokhrel and K. S. Nagaraja, *Phys. Stat. Sol. A* 198, 343 (**2003**).
58. I. C. Cosentino, E. N. S. Muccillo, and R. Muccillo, *Sens. Actuators B* 96, 677 (**2003**).
59. J. Wang, F. Q. Wu, K. H. Shi, X. H. Wang, and P. P. Sun, *Sens. Actuators B* 99, 586 (**2004**).
60. P. M. Faia, C. S. Furtado, and A. J. Ferreira, *Sens. Actuators B* 101, 183 (**2004**).
61. A. M. Edwin Suresh Raj, C. Mallika, K. Swaminathan, O. M. Sreedharan, and K. S. Nagaraja, *Sens. Actuators B* 81, 229 (**2002**).
62. A. M. Edwin Suresh Raj, C. M. Magdalane, and K. S. Nagaraja, *Phys. Stat. Sol. A* 191, 230 (**2002**).
63. R. Sundaram and K. S. Nagaraja, *Sens. Actuators B* 101, 353 (**2004**).
64. Y. C. Yeh and T. Y. Tseng, *IEEE Transactions on Components, Package and Manufacturing Technology* 12, 259 (**1989**).

65. R. Sundaram, E. S. Raj, and K. S. Nagaraja, *Sens. Actuators B* 99, 350 **(2004)**.
66. Y. D. Lu, J. L. Zhang, B. R. Li, and W. Y. Pan, *Proc. Electronic Components and Technology Conference* 1991, 261 **(1991)**.
67. R. Sundaram and K. S. Nagaraja, *Sens. Actuators B* 101, 353 **(2004)**.
68. N. Rezlescu, E. Rezlescu, C. L. Sava, F. Tudorache, and P. D. Popa, *Cryst. Res. Technol.* 39, 548 **(2004)**.
69. G. Neri, A. Bonavita, C. Milone, A. Pistone, and S. Galvagno, *Sens. Actuators B* 92, 326 **(2003)**.
70. W. Qu, Q. Wlodarski, and J. U. Meyer, *Sens. Actuators B* 64, 76 **(2000)**.
71. J. Ying, C. Wan, and P. He, *Sens. Actuators B* 62, 165 **(2000)**.
72. J. Yuk and T. Troczynski, *Sens. Actuators B* 94, 290 **(2003)**.
73. A. Bearzotti, J. M. Bertolo, P. Innocenzi, P. Falcaro, and E. Traversa, *J. European Ceramic Society* 24, 1969 **(2004)**.
74. Z. A. Ansari, T. G. Ko, and J.-H. Oh, *Surface and Coating Technology* 179, 182 **(2004)**.
75. D. G. Neri, A. Bonavita, G. Rizzo, and S. Galvagno, *J. European Ceramic Society* 24, 1435 **(2004)**.
76. K. I. Arshak and K. Twomey, *Microelectronics J.* 33, 213 **(2002)**.
77. O. K. Varghese, D. Gong, M. Paulose, K. G. Ong, C. A. Grimes, and E. C. Dickey, *J. Mater. Res.* 17, 1162 **(2002)**.
78. J. Barkauskas, *Talanta* 44, 1107 **(1997)**.
79. H. Wang, C. D. Feng, S. L. Sun, C. U. Segre, and J. R. Stetter, *Sens. Actuators B* 40, 211 **(1997)**.
80. P. G. Su, I. C. Chen, and R. J. Wu, *Anal. Chim. Acta* 449, 103 **(2001)**.
81. J. Wang, B. K. Xu, S. P. Ruan, and S. P. Wang, *Mater. Chem. Phys.* 78, 746 **(2003)**.
82. J. Wang, Q. Lin, R. Zhou, and B. Xu, *Sens. Actuators B* 81, 248 **(2002)**.
83. Y. Sakai, Y. Sadaoka, and H. Fukumoto, *Sens. Actuators* 13, 243 **(1988)**.
84. Y. Sakai, Y. Sadaoka, M. Matsuguchi, and H. Sakai, *Sens. Actuators B* 24, 689 **(1995)**.
85. Y. Sakai, Y. Sadaoka, and M. Matsuguchi, *Sens. Actuators B* 35, 85 **(1996)**.
86. Y. Sakai, M. Matsuguchi, and T. Hurukawa, *Sens. Actuators B* 66, 135 **(2000)**.
87. M. S. Gong, S. W. Joo, and B. K. Choi, *Sens. Actuators B* 86, 81 **(2002)**.
88. S. Y. Son and M. S. Gong, *Sens. Actuators B* 86, 168 **(2002)**.
89. Y. Li and M. J. Yang, *Sens. Actuators B* 87, 184 **(2002)**.
90. I. Fratoddi, P. Altamura, A. Bearzotti, A. Furlani, and M. V. Russo, *Thin Solid Films* 458, 292 **(2004)**.
91. Y. Li and M. J. Yang, *Sens. Actuators B* 86, 155 **(2002)**.
92. M. S. Gong, J. S. Park, M. H. Lee, and H. W. Rhee, *Sens. Actuators B* 86, 160 **(2002)**.
93. C. W. Lee, H. W. Rhee, and M. S. Gong, *Sens. Actuators B* 73, 124 **(2001)**.
94. C. W. Lee, Y. Kim, S. W. Joo, and M. S. Gong, *Sens. Actuators B* 88, 21 **(2003)**.
95. K. Suri, S. Annapoorni, A. K. Sarkar, and R. P. Tandon, *Sens. Actuators B* 81, 277 **(2002)**.
96. S. H. Park, J. S. Park, C. W. Lee, and M. S. Gong, *Sens. Actuators B* 86, 68 **(2002)**.
97. M. J. Yang, Y. Li, N. Camaioni, G. Casalbore-Miceli, A. Martelli, and G. Ridolfi, *Sens. Actuators B* 86, 229 **(2002)**.
98. A. Bearzotti, J. M. Bertolo, P. Innocenzi, P. Falcaro, and E. Traversa, *Sens. Actuators B* 95, 107 **(2003)**.
99. J. M. Ingram, M. Greb, J. A. Nicholson, and A. W. Fountain III, *Sens. Actuators B* 96, 283 **(2003)**.
100. Y. Li, M. J. Yang, and Y. She, *Talanta* 62, 707 **(2004)**.
101. W. Wang and A. V. Virkar, *Sens. Actuators B* 98, 282 **(2004)**.
102. P. G. Su and W. Y. Tsai, *Sens. Actuators B* 100, 417 **(2004)**.
103. C. W. Lee, O. Kim, and M. S. Gong, *J. Applied Polymer Science* 89, 1062 **(2003)**.
104. V. G. Litovchenko, T. I. Gorbanyuk, V. S. Solntsev, and A. A. Evtukh, *Appl. Surf. Sci.* 234, 262 **(2004)**.
105. L. J. Golonka, B. W. Licznerski, K. Nitsch, and H. Teterycz, *Meas. Sci. Technol.* 8, 92 **(1997)**.
106. A. Schroth, K. Sager, G. Gerlach, A. Häberli, T. Boltshauser, and H. Baltes, *Sens. Actuators B* 34, 301 **(1996)**.
107. R. Buchhold, A. Nakladal, G. Gerlach, and P. Neumann, *Sens. Actuators B* 53, 1 **(1998)**.
108. K. Sager, G. Gerlach, and A. Schroth, *Sensors Materials* 6, 333 **(1994)**.
109. K. Sager, G. Gerlach, A. Nakladel, and A. Schroth, *Sens. Actuators A* 46, 171 **(1995)**.
110. K. Sager, A. Schroth, A. Nakladal, and G. Gerlach, *Sens. Actuators A* 53, 330 **(1996)**.
111. J. M. Barandiaran and J. Gutierrez, *Sens. Actuators A* 59, 38 **(1997)**.
112. J. M. Barandiaran, J. Gutierrez, and C. Gómez-Polo, *Sens. Actuators* 81, 154 **(2000)**.
113. P. G. Stoyanov and C. A. Grimes, *Sens. Actuators* 80, 8 **(2000)**.
114. C. A. Grimes and D. Kouzoudis, *Sens. Actuators* 84, 205 **(2000)**.
115. C. A. Grimes, K. G. Ong, K. Loiselle, P. G. Stoyanov, D. Kouzoudis, Y. Liu, C. Tong, and F. Tefiku, *J. Smart Mater. Struct.* 8, 639 **(1999)**.
116. E. D. T. de Lacheisserie, *J. Magn. Magn. Mater.* 25, 251 **(1982)**.
117. K. E. Heusler, A. Grzegorzewski, L. Jackel, and J. Pietrucha, *Deut. Bunsenge. Phys. Chem.* 92, 1218 **(1988)**.
118. C. A. Grimes, D. Kouzoudis, and C. Mungle, *Rev. Sci. Instrum.* 7, 3822 **(2000)**.
119. S. Schmidt and C. A. Grimes, *Sens. Actuators A* 94, 189 **(2001)**.
120. Q. Y. Cai, M. K. Jain, and C. A. Grimes, *Sens. Actuators B* 77, 614 **(2001)**.
121. Q. Y. Cai, A. Cammers-Goodwin, and C. A. Grimes, *J. Environ. Monitoring* 2, 556 **(2000)**.
122. Q. Y. Cai and C. A. Grimes, *Sens. Actuators B* 71, 112 **(2000)**.
123. Q. Y. Cai and C. A. Grimes, *Sens. Actuators B* 79, 144 **(2001)**.
124. C. A. Grimes, D. Kouzoudis, E. C. Dickey, D. Qian, M. A. Anderson, R. Shahidain, M. Lindsey, and L. Green, *J. Appl. Phys.* 87, 5341 **(2000)**.
125. A. F. Cobeño, A. P. Zhukov, E. Pina, J. M. Blanco, J. Gonzalez, and J. M. Baradiaran, *J. Magn. Magn. Mater.* 215, 743 **(2000)**.
126. C. Y. Lee and G. B. Lee, *J. Micromech. Microeng.* 13, 620 **(2003)**.